J. Fluid Mech. (1998), *vol.* 371, *pp.* 157–178. Printed in the United Kingdom

© 1998 Cambridge University Press

Low-dimensional control of the circular cylinder wake

By E. A. GILLIES

Department of Aerospace Engineering, University of Glasgow, Glasgow, UK

(Received July 2 1997 and in revised form 27 April 1998)

Many wake flows exhibit self-excited flow oscillations which are sustained by the flow itself and are not caused by amplification of external noise. The archetypal example of a self-excited wake flow is the low Reynolds number flow past a circular cylinder. This flow exhibits self-sustained periodic vortex shedding above a critical Reynolds number. In general, control of such flows requires stabilization of many globally unstable modes; the present work describes a multiple-sensor control strategy for the cylinder wake which succeeds in controlling a simplified wake model at a Reynolds number above that at which single-sensor schemes fail.

Representation of the flow field by a finite set of coherent structures or modes, which are extracted by proper orthogonal decomposition and correspond to the large-scale wake components, allows the efficient design of a closed-loop control algorithm. A neural network is used to furnish an empirical prediction of the modal response of the wake to external control forcing. This model avoids the need for explicit representation of the control actuator–wake interaction. Additionally, the neural network structure of the model allows the design of a robust nonlinear control algorithm. Furthermore the controller does not necessarily require velocity field information, but can control the wake using other quantites (for example flow visualization pictures) which characterize the structure of the velocity field. Successful control of a simplified cylinder wake model is used to demonstrate the feasibility of the low-dimensional control strategy.

1. Introduction

Active control of unsteady separated fluid flows has attracted much interest in recent years (see, for example, Gopalkrishnan *et al.* 1994; Park, Ladd & Hendricks 1994; Roussopoulos 1993; Tokumaru & Dimotakis 1991; Tao, Huang & Chen 1996). Control of the circular cylinder wake flow, which is an archetypal unstable flow, has received a large amount of attention because of a wide range of aeronautical, civil, mechanical and chemical engineering applications – ranging from noise and vibration control, chemical mixing improvement, dynamic stall control and lift enhancement (Cortelezzi, Leonard & Doyle 1994; Cortelezzi 1996).

Above a critical Reynolds number, the wake of a circular cylinder exhibits vortex shedding oscillations which persist purely as a result of flow instability and which are not due to the influence of external forcing, noise, or internal pressure feedback. The flow exhibits *self-excited oscillations* and this has important consequences for flow control. A significant region of *absolute* instability is present in the near wake and is a necessary condition for self-excited, global wake oscillations (Karniadakis &

https://doi.org/10.1017/S0022112098002122 Published online by Cambridge University Press

Triantafyllou 1989; Huerre & Monkewitz 1990). For a comprehensive review of the wake see Williamson (1996).

1.1. *Response of self-excited cylinder wakes to external control*

The response of the cylinder flow, and absolutely unstable wake flows in general, to periodic forcing above a threshold amplitude has the characteristics of a nonlinear oscillator with forced oscillations (Detemple-Laake & Eckelmann 1989). The response of a circular cylinder wake to open loop forcing can be characterized by two qualitatively different regimes, 'lock-in' and 'beat', which are dependent on the frequency content of the applied forcing (Karniadakis & Triantafyllou 1989; Detemple-Laake & Eckelmann 1989).

Several different forcing techniques affect the behaviour of the cylinder flow; however, the wake response to forcing is similar for each, whether acoustic excitation of the wake (Detemple-Laake & Eckelmann 1989; Roussopoulos 1993), longitudinal or lateral vibration of the cylinder (Detemple-Laake & Eckelmann 1989), rotation of the cylinder (Tokumaru & Dimotakis 1991), alternate blowing and suction at the separation points (Roussopoulos 1993) or (for low Reynolds numbers) vibrating wires in the wake (Karniadakis & Triantafyllou 1989) are used. All of these methods have been proposed for vortex shedding suppression schemes: active control schemes involving rotation of the cylinder (Tokumaru & Dimotakis 1991) or alternate asymmetric suction/blowing (Lewit 1992) have met with some success. Open loop control of a cylinder wake by means of an oscillating aerofoil placed in the near wake has also been used to alter the position and strength of large-scale vortex structures in the wake (Gopalkrishnan *et al.* 1994). These controllers inject circulation into the flow; but there is a *nonlinear* interaction between the global modes and the control input (Schumm, Berger & Monkewitz 1994).

For convectively unstable flows, a linear stability analysis reveals the receptivity of the flow to external forcing at various frequencies: out-of-phase, sinusoidal forcing at the same frequency as the dominant Fourier component of the instability wave can, in theory, stabilize a convectively unstable flow (such as a boundary layer, Metcalfe *et al.* 1986). Control of global flow oscillations that are the result of absolute instability, as in the circular cylinder wake, is more difficult. Although the von Kármán mode is the first global mode to become unstable, a wake flow may possess multiple global modes. Control of the flow requires attenuation of all of these global modes (Monkewitz 1989). At values of the Reynolds number just above the critical value for self-excited oscillations, there is typically only one globally unstable mode, resulting in Kármán vortex shedding (Huerre & Monkewitz 1990); therefore the flow behaviour at each point in the wake is related to every other by a simple phase shift (Park *et al.* 1994). Linear feedback control of such flows is therefore, theoretically, possible by means of a *single* sensor-actuator feedback loop. Indeed, single-sensor control of such low Reynolds number cylinder wakes has been observed experimentally (Park *et al.* 1994; Ffowcs-Williams & Zhao 1989; Roussopoulos 1993). At higher values of the relevant flow parameter, however, other global modes are present. Nevertheless, at only slightly supercritical Reynolds numbers ($Re < 60$ from tunnel experiments of Roussopoulos (1993) or $Re < 80$ in a numerical experiment of Park *et al.* (1994)) there often exists a 'gain window' between the threshold amplitudes for the global modes, such that forcing with an amplitude large enough to suppress the most unstable mode is still not large enough to destabilize the next global mode. Complete suppression or control of the wake is therefore still feasible using a single sensor at these slightly supercritical Reynolds numbers, although there may exist multiple global modes (Park *et al.* 1994).

https://doi.org/10.1017/S0022112098002122 Published online by Cambridge University Press

Further beyond the critical value, however, the 'gain window' shrinks so that the forcing amplitude necessary to control the most unstable mode merely destabilizes the next most unstable mode (Roussopoulos 1993; Monkewitz 1989). Oscillations may be suppressed at the sensor location (Ffowcs-Williams & Zhao 1989) but are, in general, exacerbated elsewhere (Roussopoulos 1993). *Points in the wake are therefore not merely connected via a phase shift and so multiple, spatially distributed sensors are needed for control of the flow.*

1.2. *Low-dimensional control of self-excited cylinder wakes*

The presence of multiple global modes in the absolutely unstable cylinder wake necessitates the use of multiple control sensors at various streamwise locations for the suppression of all possible modes (Gopalkrishnan *et al.* 1994; Monkewitz 1989). The spatio-temporal response of the wake is nonlinear: a control strategy, based on a nonlinear model of the flow dynamics is therefore appropriate (Lightbody, Wu & Irwin 1992).

If the absolutely unstable region is to be adequately represented with multiple control sensors, then many flow variables (for example velocity or pressure) at many points throughout the unstable region are needed within the feedback or control algorithm. The resulting control algorithm involves many variables and will therefore be complicated and computationally slow. If, however, the complex spatio-temporal information, needed for nonlinear feedback stabilization of multiple global modes, is characterized by a relatively small number of quantities, given by a low-dimensional description of the flow features and their response to external forcing, then it is reasonable to assert that the feedback control algorithm can be made simpler and computationally feasible (Gillies & Anderson 1994; Cortelezzi 1996). Typically, cylinder wake flows are dominated by the dynamics of large-scale spatial structures; the dynamics of small-scale spatial structures are relatively unimportant in the evolution of these flows. Physical evidence supports the idea that at least periodically forced, absolutely unstable flows can be regarded as low-dimensional. For example, a relatively small number of characteristic spatial structures are observed in experimental periodically forced vortex streets (for example, twelve spatial modes have been observed during large-amplitude acoustic excitation of a cylinder wake by Detemple-Laake & Eckelmann (1989); alternatively, three spatial interaction modes have been observed behind a cylinder with an oscillating aerofoil in the near wake by Gopalkrishnan *et al.* (1994)). It is likely that a wake flow will remain low-dimensional as long as the forcing input is not too large and the flow is not excited into a higher dimension state (e.g. with very large control inputs the wake may become three-dimensional) (Ohle & Eckelmann 1992). A control strategy that is restricted to measurement and control of just a finite number of large-scale spatial structures in the cylinder wake is potentially simpler than a control scheme which attempts to control both the large and small scales of the flow. A control strategy restricted to large-scale spatial structures is still, however, able to control the most important features of the wake oscillations.

1.3. *Scope of the paper*

It is reasonable to assert that control of the two-dimensional wake must be demonstrated before three-dimensional instabilities are addressed (Schumm *et al.* 1994). This paper is specific to the low Reynolds number, laminar, two-dimensional cylinder wake (the regular range persists up to $Re \simeq 194$ (Williamson 1996); however, with synchronized forcing along the span, as say, by cylinder rotations, or by acoustic excitation,

https://doi.org/10.1017/S0022112098002122 Published online by Cambridge University Press

the regular two-dimensional range can persist up to $Re \simeq 450$ (Detemple-Laake & Eckelmann 1989)), although much of the strategy is generic. A simulation of wake control is demonstrated on a wake model at $Re = 100$: this Reynolds number is above the value where single-sensor linear control schemes fail to suppress all of the global modes.

Focusing on the laminar two-dimensional wake is advantageous because numerical simulation of this wake is readily implemented: in numerical simulations all flow variables are available for analysis without the use of intrusive sensors and control system computations may be performed in *virtual* time.

Section 2 describes the utility of the proper orthogonal decomposition (POD) as a low-dimensional model of the spatial structures in the wake forced by a control actuator (as measured by spatially distributed sensors). The third section describes how a mapping between parameters of an actual, physical control actuator and the response of the POD modes is automatically accounted for by an empirical neural network. This section also describes how this neural prediction leads to a nonlinear control algorithm to drive the control actuator. The fourth section is a demonstration of the scheme on a simplified wake simulation at $Re = 100$.

2. The method of proper orthogonal decomposition

It is appropriate to search for some readily identifiable coordinate basis that spans the large-scale components of the wake (at, say, a particular Reynolds number). Such a basis is furnished by proper orthogonal decomposition (POD). For a comprehensive review of POD see Holmes, Lumley & Berkooz (1996). The method is slightly altered here to account for the non-stationary effects of time-dependent control forcing.

It is readily shown that characteristic features, $\boldsymbol{\psi}$, of the flow correspond to eigen-solutions of the time-average, spatial correlation matrix, $\boldsymbol{R}$, of the fluctuating velocity field, $\boldsymbol{V}'$,

$$\boldsymbol{R} = E\{\boldsymbol{V}'(t)\boldsymbol{V}'(t)^T\}. \tag{1}$$

If the POD modes are to be representative of the wake during a control run, the modes must be extracted from the wake when forced by a suitable control actuator. Statistical properties of the wake forced by a time-dependent control will be non-stationary. The POD is therefore extended (following Glezer, Kadioglu & Pearlstein (1989)). N disjoint time series, containing M snapshots of the flow velocity field each, are assembled from forced wake measurements. The wake should be forced at different amplitudes and frequencies (as in Detemple-Laake & Eckelmann 1989) or by using a 'chirp' signal to ensure that a wide range of POD modes are excited. If N different flow transients during forcing of the flow are examined, then a concatenated matrix may be formed – an intelligent choice of first and last points in each series might be, for example, the start and finish points of one period of a forcing cycle because no further information is gained from analysis of further forcing cycles. The correlation matrix for POD expansion of the non-stationary data is formed from the concatenated data matrix and is the *average of the correlations from each distinct example of forcing* (Glezer *et al.* 1989):

$$\boldsymbol{R} = \frac{1}{N}\sum_{i=1}^{N}\boldsymbol{R}_i. \tag{2}$$

At any time, the velocity field can be reconstructed approximately from a *linear*

https://doi.org/10.1017/S0022112098002122 Published online by Cambridge University Press

combination of the mean flow and a finite number of modes.

$$\boldsymbol{V}(t) \approx \overline{\boldsymbol{V}} + \sum_{i=1}^{M} A_i(t)\boldsymbol{\psi}_i \tag{3}$$

where the modal amplitude

$$A_i(t) = (\boldsymbol{\psi}_i \cdot \boldsymbol{V}'(t)). \tag{4}$$

The sum of the eigenvectors is proportional to the mean energy of the fluctuating velocity field. If the velocity field is reconstructed using only the modes corresponding to the N largest eigenvalues, then the proper orthogonal decomposition captures more of the flow kinetic energy for a given N than any other expansion (Glezer *et al.* 1989).

It is reasonable to assert that a finite representation of the wake by sub-optimal POD modes generated from a large enough non-stationary data ensemble is possible (Glezer *et al.* 1989): acoustically forced wakes show only a small number (twelve) of qualitatively different spatial modes (Detemple-Laake & Eckelmann 1989). When considering the number of time-series required for complete characterization of the flow (rather than just one set of observed phenomena), the type of forcing is also of interest. A comparison between the effects of harmonic and an-harmonic forcing for a plane mixing layer in (Glezer *et al.* 1989) shows that the wake structures do not significantly differ between the two forcing regimes. Therefore, modes developed from one forcing regime are useful for other types of forcing, such as feedback (Glezer *et al.* 1989) (the behaviour of forced cylinder wakes is also relatively insensitive to the exact character of forcing (Roussopoulos 1993; Detemple-Laake & Eckelmann 1989)). For this statement to apply generally, more experimental evidence is required, but the similarity of the modes generated during two different forcing regimes of the mixing layer is encouraging.

3. Control of large-scale wake structures

3.1. *Introduction of control terms into a prediction of the flow dynamics*

Comparison of various forcing techniques has shown that the injection of circulation into the wake is a common mechanism by which the wake can be controlled (Tokumaru & Dimotakis 1991; Schumm *et al.* 1994). This may be achieved by lateral cylinder vibrations (Detemple-Laake & Eckelmann 1989), cylinder rotations (Tokumaru & Dimotakis 1991) or alternate suction and blowing (Roussopoulos 1993) or flapping foils in the near wake (Gopalkrishnan *et al.* 1994). Alternatively, the cylinder wake is also sensitive to acoustic forcing (Ffowcs-Williams & Zhao 1989). All of these control actuations produce similar wake responses and all are able to promote sub-critical vortex shedding. The nonlinear interaction between control inputs, provided by such actuators, and the global modes of the flow have, however, eluded explanation (Schumm *et al.* 1994). For control of two-dimensional oscillations there are several qualitatively similar choices for control actuator. For three-dimensional wakes (at $Re > 194$ in Williamson 1996), acoustic excitation at one point along the span has too small an amplitude to influence oscillations at other spanwise locations (Roussopoulos 1993). However, for 3D wake control, active cylinder rotations may hold more promise (Tokumaru & Dimotakis 1991): for this type of actuation, the forced shedding mechanism replaces the natural mechanism and the actuation is constant along the span.

https://doi.org/10.1017/S0022112098002122 Published online by Cambridge University Press

Say a particular actuator is chosen for controlling the wake. Following the extended POD method of Glezer *et al.* (1989), in § 2, a finite set of POD modes is obtained from observations of the cylinder wake velocity field forced by the control actuator. For the design of a control algorithm, which will drive the actuator, a prediction of the response of the mode amplitudes (and hence, the flow) to control forcing is useful. The control problem is to drive the actuator so that the observed mode amplitudes correspond to a desired flow condition. A finite-dimensional dynamical model of the flow may be obtained from classical Galerkin approximation of the Navier–Stokes equations. However, the general form of the evolution equation for the mode amplitudes in the presence of the control input is

$$\frac{\mathrm{d}A_k}{\mathrm{d}t} = G_k^c\,(A_1, A_2, \ldots, A_M, u_1(t), \ldots, u_c(t)), \qquad k = 1, \ldots, M, \tag{5}$$

where the $u_i(t)$ are the time-dependent controls. The functional form of G_k^c depends implicitly on the physical interaction of the control input with the flow field; this interaction has been observed to be a nonlinear process. The effect of the physical control actuator may be introduced by direct analytical manipulation of the Navier–Stokes equations. However, mapping the effects of a physical control actuator from velocity field space to POD mode space (see, for instance, Berkooz, Psiaki & Fischer (1994)) may be a complicated process, especially for control actuators that are geometrically complex or otherwise difficult to model: e.g. multiple actuators, acoustic excitation, flapping foils. The rational addition of terms in the classical Galerkin approximation resulting from an actual physical control may therefore be very difficult. An alternative approach is suggested here which circumvents the need for direct manipulation of the Navier–Stokes equations by automatically introducing physical control terms with a neural network. Moreover, the neural network prediction of the flow to control forcing proves ultimately useful for designing a control algorithm.

If the observed response of the wake (and hence the observed mode amplitudes) to parameters of an actual control actuator is recorded from an experiment, then the physical control–mode interaction may be estimated empirically by a neural network. The neural network is trained to predict the observed response of the POD modes from physical actuation of the velocity field in an experiment. In this way, the nonlinear mapping between physical controller parameters (such as actuation frequency and amplitude) and the temporal behaviour of the (forced) wake in POD space is automatically accounted for.

3.2. *Neural network emulation of the forced wake*

To emulate the fluid mode amplitude evolution a static (multi-layer perceptron) neural network is chosen. This choice proves advantageous for the design of a control algorithm. The reduced-order flow model (5) is represented by an equivalent discrete-time process described by a nonlinear regressive model of order p (Hush & Horne 1993),

$$\boldsymbol{A}(n+1) = \Gamma\,(\boldsymbol{A}(n), \boldsymbol{A}(n-1), \ldots, \boldsymbol{A}(n-p), \boldsymbol{u}(n), \ldots, \boldsymbol{u}(n-p)) \tag{6}$$

where $\boldsymbol{A}(n) = (A_1(n), A_2(n), \ldots, A_M(n))$ and $\boldsymbol{u}(n) = (u_1(n), u_2(n), \ldots, u_c(n))$. The relationship between present, past and future flow state is predicted (for each discrete time step) as the network is continually supplied with the actual present and past flow states. The neural emulator then has the form of a one-step predictor,

$$\hat{\boldsymbol{A}}(n+1) = \hat{\Gamma}\,(\boldsymbol{A}(n), \boldsymbol{A}(n-1), \ldots, \boldsymbol{A}(n-p), \boldsymbol{u}(n), \ldots, \boldsymbol{u}(n-p)) \tag{7}$$

https://doi.org/10.1017/S0022112098002122 Published online by Cambridge University Press

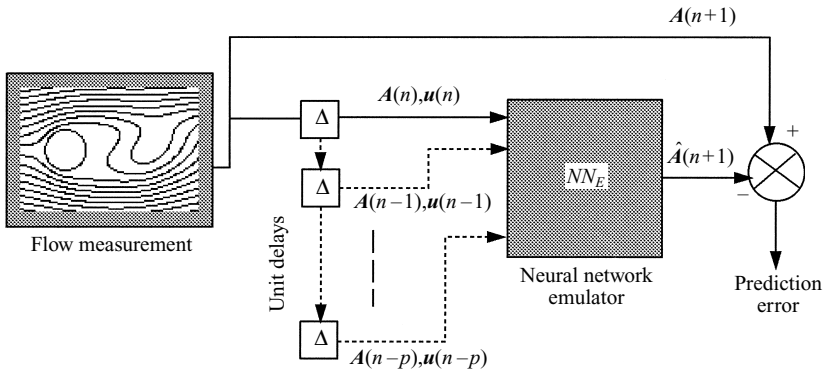


FIGURE 1. Neural emulator: one-step predictor.

which is trained to minimize the magnitude of the error vector

$$\boldsymbol{e} = (\boldsymbol{A}(n+1) - \hat{\boldsymbol{A}}(n+1)). \tag{8}$$

Error values do not accumulate, because there is no feedback in the static network, and so the network can be trained to provide a very accurate prediction of the future fluid state. A multi-layer perceptron, used as a one-step predictor, to emulate the nonlinear response of the fluid to a control input is shown schematically in figure 1. The network is trained by recursive adjustment of the connection strengths in the network by the *backpropagation algorithm*, which is an error gradient descent technique designed to minimize the mean-squared error of the output (Haykin 1994; Hush & Horne 1993). The local error gradient at each node of the network is computed by backpropagation of the network error from the output (where the error is the difference between the actual and the desired network response) back to the input.

3.3. *Nonlinear control*

The neural emulator of the flow dynamics provides a prediction of the fluid state, given initial mode amplitude conditions and values for external control parameters. The predicted response of the fluid is used to design a controller, such that the predicted response to an applied control minimizes the control system error and the flow is driven towards a desired state.

If the neural emulator is fed a control input (for example, the amplitude and frequency of actuation), it will provide predicted values for the mode amplitudes in response to actuation at the next time step (Nguyen & Widrow 1990).

$$\boldsymbol{u}(n), \boldsymbol{A}(n) \rightarrow \hat{\boldsymbol{A}}(n+1). \tag{9}$$

The difference between the predicted amplitudes, $\hat{\boldsymbol{A}}$, and the desired set of amplitudes, $\boldsymbol{A}_d$, for the control system is the *control system error vector*,

$$\boldsymbol{e}_{CS} = (\boldsymbol{A}_d(n+1) - \hat{\boldsymbol{A}}(n+1)). \tag{10}$$

This error does not, however, directly reveal the *error in the applied control*,

$$\boldsymbol{e}_u = (\boldsymbol{u}^g(n) - \boldsymbol{u}(n)), \tag{11}$$

where $\boldsymbol{u}^g$ is the unknown control that would either provide a control system error of zero magnitude (the $\boldsymbol{u}^g$ applied to $\boldsymbol{A}(n)$ such that $|(\boldsymbol{A}_d(n+1) - \hat{\boldsymbol{A}}(n+1))| = 0$), or

https://doi.org/10.1017/S0022112098002122 Published online by Cambridge University Press

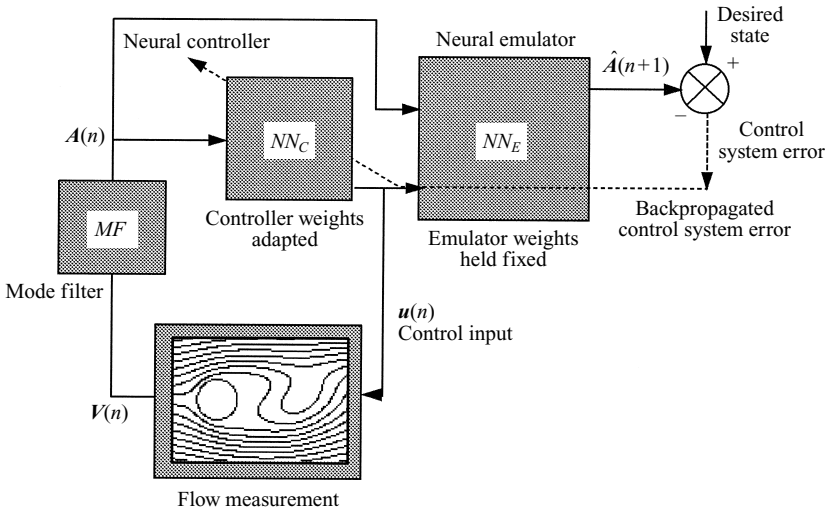


FIGURE 2. Nonlinear control of fluid flow.

the unknown control that would make the magnitude of the control system error less than the previous value (the $\boldsymbol{u}^g$ applied to $\boldsymbol{A}(n)$ such that $|(\boldsymbol{A}_d(n+1) - \hat{\boldsymbol{A}}(n+1))| < |(\boldsymbol{A}_d(n) - \hat{\boldsymbol{A}}(n))|$). The error in the applied control, rather than the control system error, is necessary to adjust the control to provide the desired fluid response at the next time step (Lightbody *et al.* 1992; Jacobson & Reynolds 1993).

The error in the applied control is, however, available by backpropagation of the control system error vector, through the emulator, to the control inputs because the *emulator is a neural network* (Lightbody *et al.* 1992; Jacobson & Reynolds 1993; Nguyen & Widrow 1990). The control system error, backpropagated through the emulator with its weights held fixed, is used to train a controller neural network to apply a suitable control input to the flow (Nguyen & Widrow 1990). The error gradient at a controller network output node is treated like an error gradient of an internal hidden node – as if the controller and emulator are one network (Jacobson & Reynolds 1993). The controller weights are updated by further backpropagation through the controller so that a better control input is provided at the next time step. The neural control process is shown, schematically, in figure 2. This type of control is very robust to external perturbations (Lightbody *et al.* 1992) because the control algorithm (defined by the controller weights) is updated at each time step (so the control is adaptive). The control is a combination of either nonlinear or linear feedback of the present mode amplitudes and a nonlinear function of the control system error, depending on whether the controller network is nonlinear or linear,

$$\boldsymbol{u}(n) = \boldsymbol{f}(\boldsymbol{A}(n)) + \boldsymbol{g}(\boldsymbol{A}(n) - \hat{\boldsymbol{A}}(n)) \tag{12}$$

where $\boldsymbol{f}$ is a function of the controller network, and $\boldsymbol{g}$ is a function of the emulator network. The neural control scheme, therefore provides a nonlinear control that drives the fluid state towards a desired combination of mode amplitudes, without explicit modelling of the effect of the control on the flow field or recourse to complicated multi-variable nonlinear control theory (Jacobson & Reynolds 1993). The controller

https://doi.org/10.1017/S0022112098002122 Published online by Cambridge University Press

does not require an inverse of the emulator mapping to exist and will drive the system state closer to the control goal irrespective of the existence of an inverse model of the flow dynamics.

3.4. *Neural estimation of the POD modes*

The emulation and subsequent control of the fluid flow is encapsulated within the empirical neural network framework. The extraction of the POD modes is also an empirical process, and can therefore be rearranged into a neural network format to provide continuity within the modelling and control scheme. Recursive estimation of the POD modes avoids the need for storage and calculation of a potentially large correlation matrix and also avoids the need for direct numerical calculation of the correlation eigenproblem. The POD method is a linear decomposition and can therefore be performed by a neural network consisting of only a single layer of linear neurons (Haykin 1994).

This network then acts as a linear filter that extracts the mode amplitudes from an examination of the flow field, performing the calculation of equation (6). The mode amplitude filter, which has the structures of the POD modes contained in its weights, is implemented in the control scheme as shown in figure 2. The controller is fed a measurement of the flow field, from which it calculates the mode amplitudes, a control output and a predicted response. The control output is applied to the actual flow.

3.5. *Control sensors*

It is likely that complete suppression of global flow oscillations in the two-dimensional wake necessitate the use of multiple sensors – ideally a 'picture' of the flow field in response to control actuation. This poses no difficulty in a computational scheme (as is considered in this paper), where the entire velocity field is available. However, if the control strategy is to be implemented in an experiment then it is unlikely that the entire velocity field could be measured. Velocities at various spatial locations could, in an experiment, be obtained from a hot-wire rake (as in Glezer *et al* (1989)). From the results of Roussopoulos (1993) it seems that hot wires for controlling the flow should be placed within the absolutely unstable region (i.e. within 5 cylinder diameters of the cylinder). Arrangements of hot wires used as control sensors, placed at different streamwise locations, may increase the 'controllable' range of Reynolds numbers.

For higher Reynolds number flows, there are many global modes: this may necessitate using more sensors than can be practically implemented with intrusive hot wires. Non-intrusive methods of velocity-field measurement require seeding the flow. PIV, for instance, could obtain a velocity field 'picture'; however, the pre-processing required makes the use of this technique difficult for implementation in a control scheme.

In the strategy outlined in this paper, the temporal response of the flow is predicted using a neural network. This network does not necessarily require the POD modes to be constructed from the velocity field (unlike in a Galerkin approximation). Instead, any flow structure in the wake which can be used to indicate the presence of vortex shedding can be used to generate POD modes. For example, POD modes could be extracted from grey-scale CCD pictures of a wake flow seeded with particles. A neural emulator could then estimate the response of these visual flow structures (which are indicative of the vortex shedding response) to control actuation. The passage of smoke structures could be used to indicate the global modes in the wake (see, for instance the smoke pictures in Schumm *et al.* (1994), or the grey-scale pictures of

https://doi.org/10.1017/S0022112098002122 Published online by Cambridge University Press

aluminium flakes extracted in Gopalkrishnan *et al.* (1994) and Williamson (1996)); direct velocity field measurements are not required. As long as flow visualization structures, such as smoke patterns, are observed when they are close to the cylinder (in or near the absolutely unstable region) then they correspond closely to actual structure in the velocity field (farther downstream, smoke structures can persist, even when no coherent vortex structures exist in the velocity field (Holmes *et al.* 1996)).

4. A prototype wake control problem

To illustrate the utility of the low-dimensional control method the unsteady velocity field of a low Reynolds number, two-dimensional cylinder wake is simulated. The cylinder flow is simulated numerically, so that the entire velocity field is available for analysis. The velocity fields at various points in time in a wake transient (during the unforced growth of oscillations) are used to form a characterization ensemble. To characterize non-stationary flow features that are the result of a control input and also to predict the mode dynamics it is necessary that the cylinder flow is forced by a time-varying control input. To obviate the large computational costs involved in forcing the high-resolution numerical solution of the wake the response of the flow is simulated by a prototype model. Simulation of the control strategy with a full numerical solution of the forced Navier–Stokes equations is preferable for accuracy but is computationally intensive. It is appropriate that initial testing of the control strategy is employed on a simpler prototype flow so that identification of important parameters in the controller proceeds quickly (most of the computational effort required for a full numerical solution concentrates on modelling the flow itself and identification of important parameters in the controller is not straightforward) (Cortelezzi *et al.* 1994). The prototype flow is a reduced-order form of the flow equations with an artificial control input. The reduced-order prototype flow is based on a set of POD modes developed from the unforced numerical (CFD) simulation. The validity of the prototype model is discussed in this paper (both with respect to unforced flows, where a quantitative comparison with the full numerical solution can be made, and with respect to forced flows, where only a qualitative comparison between the model and experiment can be made). The prototype captures some important stability features of the unforced flow and accurately represents the spatial and temporal characteristics of the unforced flow. The prototype also mimics some of the features of the forced cylinder wake, and it can be asserted that the prototype flow is a reasonable qualitative model of the forced and unforced cylinder wake for initial testing of the control strategy. The prototype flow model can be integrated easily and is used to provide artificial, non-stationary velocity fields for characterization and subsequent control.

4.1. *Numerical solution of the laminar cylinder wake*

The cylinder flow is simulated numerically, using the commercially available, finite difference, CFD package, FLUENT v4.10. Uniform inlet velocity at a Reynolds number of 100 ensures that the wake is within the laminar vortex shedding region ($47 < Re < 250$). The turbulent wake $Re > 250$ is more difficult to simulate. The finite difference grid is 35 cylinder diameters long by 10 cylinder diameters wide and a body-fitted grid is used, comprising 6600 cells.

The power spectral density, calculated from a 512 point Hanning window of the wake velocity signals is shown in figure 3. The signal is seen to contain one dominant frequency (the vortex shedding mode) and three significant higher harmonics.

The Strouhal number calculated by the FLUENT method is 0.153 and this com-

https://doi.org/10.1017/S0022112098002122 Published online by Cambridge University Press

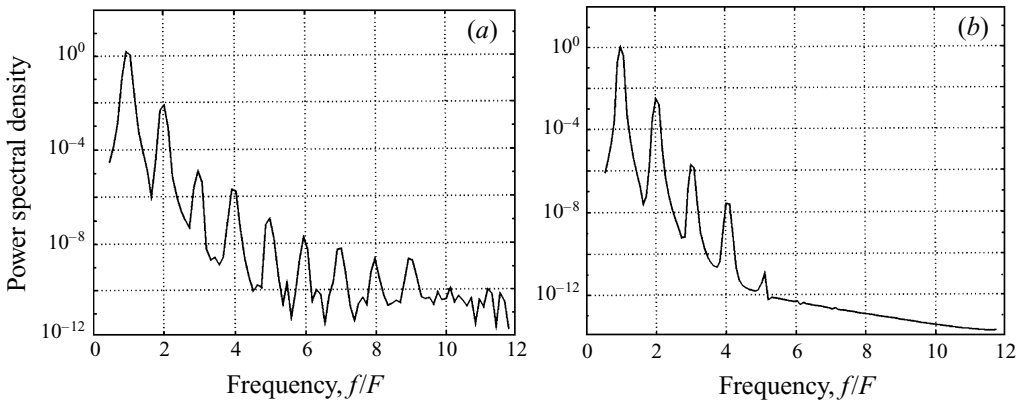


FIGURE 3. Power spectral density of velocity signal: (*a*) CFD solution, and (*b*) prototype wake.

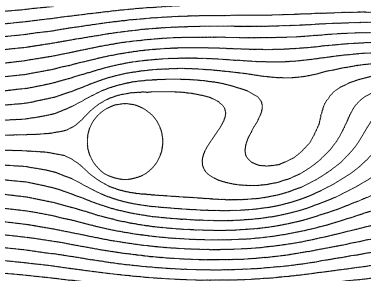


FIGURE 4. Typical instantaneous flow streamlines.

pares fairly well with those calculated by other authors (Kim & Benson 1992). The streamlines and velocity vectors obtained in the solution are also qualitatively similar to those obtained by other authors (Taylor & Morgan 1980; Kim & Benson 1992). Typical realizations of the flow streamlines during shedding are shown in figure 4.

4.2. *Simulation of a forced cylinder flow*

A prototype flow model, which has the purpose of testing the feasibility of the control scheme, is introduced here (Cortelezzi *et al.* 1994; Cortelezzi 1996). The essential properties of the prototype model are that it retains the important absolute instability features of the cylinder flow, produces qualitatively correct flow responses to forcing, and produces qualitatively correct spatial velocity fields, while remaining simple and easy to integrate.

A first approximation to modelling the forced flow is obtained by using a model of the unforced flow. A small transient of the wake is available from the unforced CFD solution. Velocity field data collected during the growth of wake oscillations, from the steady state, encapsulates wake dynamics in a neighbourhood of the unforced vortex street.

Twenty velocity fields from two flow cycles approaching the Kármán vortex street are collected. This number of snapshots is appropriate for POD characterization of such a temporally simple, laminar, unforced wake: for example, 20 POD snapshots are used in Deane *et al.* 1991 for the $Re = 100, 150$ and 200 cylinder wake and are shown to provide adequate representation of the unsteady velocity field. The ensemble average of all of the velocity fields, which approximates the time-average

https://doi.org/10.1017/S0022112098002122 Published online by Cambridge University Press

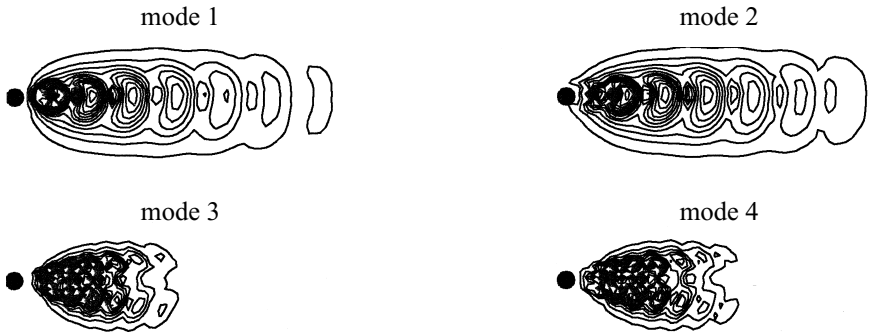


FIGURE 5. Contours of velocity magnitude of the first four POD modes.

velocity field, is calculated and subtracted from each velocity field to form twenty flow 'snapshots'. Only the first four POD modes capture significant flow energy and so the higher modes are neglected. A higher Reynolds number flow, a turbulent flow, or a time-forced flow would exhibit much richer mode composition. Contours of velocity magnitude, $(u^2+v^2)^{1/2}$, of the first four POD modes developed from the CFD data are shown in figure 5 (cf. Deane *et al.* 1991). Modes developed from double the number of snapshots (40) are similar in appearance.

A Galerkin approximation of the Navier–Stokes equations provides a succinct description of the *unforced* flow dynamics, but is difficult to establish because the Galerkin method involves spatial differentiation of the modes and mean flow and calculation of their vorticities. Numerical differentiation of the modes is difficult, and introduces error, because the modes are formed from a spatially discrete, irregular grid. The structure of the Galerkin model is, however, well documented in the literature. A transient set of velocity fields (obtained from the CFD solution during the growth of oscillations), from which the POD mode amplitudes and time derivatives at each time point are measured, can be used to fit the unknown coefficients of the quadratic Galerkin equations by least squares (rather than using a traditional Galerkin approach).

The spatial features of the cylinder flow, represented by the CFD data, are adequately approximated by just four modes. However, a four-mode quadratic model of the wake proves to be unstable (compare with Deane *et al.* 1991). Cubic terms may appear in a nonlinear Galerkin model and are introduced here to generate a stable model without adding extra modes to the four-mode prototype model.

The addition of *ad hoc* forcing terms to dynamical models of the cylinder dynamics is known to produce qualitative agreement with experiment (Ohle & Eckelmann 1992). For example, the addition of an interior sinusoidal forcing term to a low-order, cubic model of the $Re = 114$ flow past a circular cylinder produces qualitatively correct time histories and qualitatively correct regions of entrainment (Ohle & Eckelmann 1992). Simple addition of forcing terms to the least-squares developed model should also produce qualitatively correct results, and mimic the response of the flow to excitation. Obviously, a control input will affect each of the prototype mode equations by a different amount as the interaction of the control with each prototype mode depends on the spatial structure of each mode. In the Galerkin model, addition of a source term to the Navier–Stokes equations results, to a first approximation, in an extra forcing term which is the inner product of each mode with the perturbation to the velocity field from the control actuator for each mode equation, $(\psi_k \cdot f_a \boldsymbol{f}_x)$, where f_a is

https://doi.org/10.1017/S0022112098002122 Published online by Cambridge University Press

the control amplitude and $\boldsymbol{f}_x$ is the spatial distribution of the velocity resulting from the control actuator. An amplitude and spatial distribution of a localized interior control input at a coordinate (x_c, y_c) in the wake is obtained from Karniadakis & Triantafyllou 1989:

$$F(x, y, t) = f_a(t) \exp\left(-D((x - x_c)^2 + (y - y_c)^2)\right), \tag{13}$$

where D is the rate at which the contribution of the force decays with distance from the source. The position of the localized control input and the value for the decay rate is chosen such that the forcing is small at the domain boundaries and significant only in the near wake (which is necessary for control of the global modes) (Karniadakis & Triantafyllou 1989; Roussopoulos 1993). The position of the near-wake control wire is shown in figure 9. This form of control simulates an interior forcing provided by an active control device such as a vibrating wire (Karniadakis & Triantafyllou 1989). The fluid adjacent to the control device aquires an acceleration equal to the vibrating source – further from the source the acceleration decays. This distribution of control provides forcing of the near wake consistent with the boundary conditions as the amplitude of the control at the domain boundaries is very small. Vibrations of the cylinder (which are known to be suitable for control of global flow oscillations (Schumm *et al.* 1994)) give rise to a similar forcing (Karniadakis & Triantafyllou 1989). The complete form of the prototype flow model is, for $k = 1, \ldots, 4$,

$$\frac{\mathrm{d}A_k}{\mathrm{d}t} = c_o^k + \sum_{i=1}^{4} c_{1_i}^k A_i + \sum_{i=1}^{4} \sum_{j=1_{j \geqslant i}}^{4} c_{2_{ij}}^k A_i A_j + \sum_{i=1}^{4} \sum_{j=1_{j \geqslant i}}^{4} \sum_{l=1_{l \geqslant j}}^{4} c_{3_{ijl}}^k A_i A_j A_l + c_4^k f_a, \tag{14a}$$

$$\boldsymbol{V}(t) = \overline{\boldsymbol{V}} + \sum_{i=1}^{4} A_i(t) \psi_i, \tag{14b}$$

where the $A_k(t)$ are time-varying amplitudes of the first four POD modes, ψ_k, of the entire cylinder wake, established from the CFD velocity field ensemble.

The control input, although introduced somewhat artificially to the unforced prototype model, is useful because it produces temporal flow responses that are in qualitative agreement with experimental observations of forced cylinder wakes. This qualitative agreement is discussed in the next subsection. Similar models for forced wake flows are cited in the literature (Ohle & Eckelmann 1992).

4.3. *Validity of the prototype flow model*

The prototype flow model (14) consists of a spatial part (14*b*), which describes the spatial structure of the velocity field given a set of mode amplitudes, and a temporal part (14*a*), which determines the dynamical behaviour of the amplitudes. The average normalized kinetic energy error over one period of the four-mode reconstruction is low (= 0.03). The spatial structure of the unforced cylinder wake is therefore described adequately by the prototype flow model (14*b*), as long as the correct modal amplitudes are specified by (14*a*).

Given that (14*b*) adequately reconstructs the unforced velocity fields which constitute the unforced data ensemble, the validity of the temporal part of the unforced prototype flow, (14*a*), is of interest. Starting integration of the model with the mean flow, or zero mode amplitudes, as an initial condition for the velocity field should (with reference to experimental cylinder wakes) result in temporal growth of the von Kármán vortex shedding mode. The growth of oscillations is observed, in experiment, to be exponential in its linear stages, leading to limit-cycle oscillations. The growth

https://doi.org/10.1017/S0022112098002122 Published online by Cambridge University Press

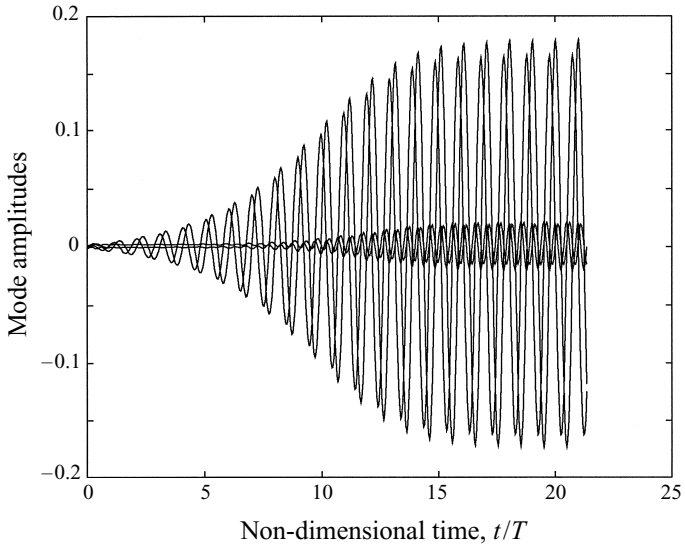


FIGURE 6. Temporal growth of unforced prototype modes.

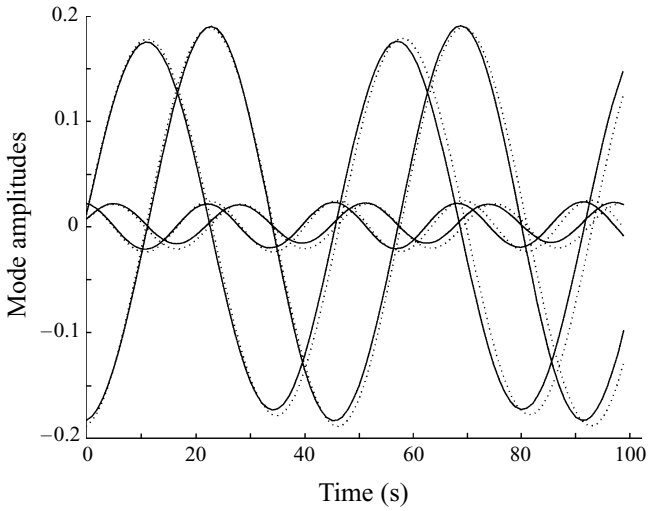


FIGURE 7. Comparison between CFD flow (dotted lines) and prototype model (solid lines): mode amplitudes on limit cycle.

of oscillations is accurately modelled by a Landau equation and the oscillations predicted by the prototype flow are, indeed, comparable to those determined by a Landau equation and those observed in experiment (Ohle & Eckelmann 1992). The growth of oscillations resulting from integration of (14*a*) are depicted in figure 6, which are typical of experimental wakes and Landau models. The qualitative nature of the instability is important for testing the feasibility of the control scheme, and the growth of instability, from the mean flow, is adequately represented by the flow prototype.

The time histories of the mode amplitudes measured from the CFD simulation and those calculated by integration of the prototype are shown in figure 7. The solid

https://doi.org/10.1017/S0022112098002122 Published online by Cambridge University Press

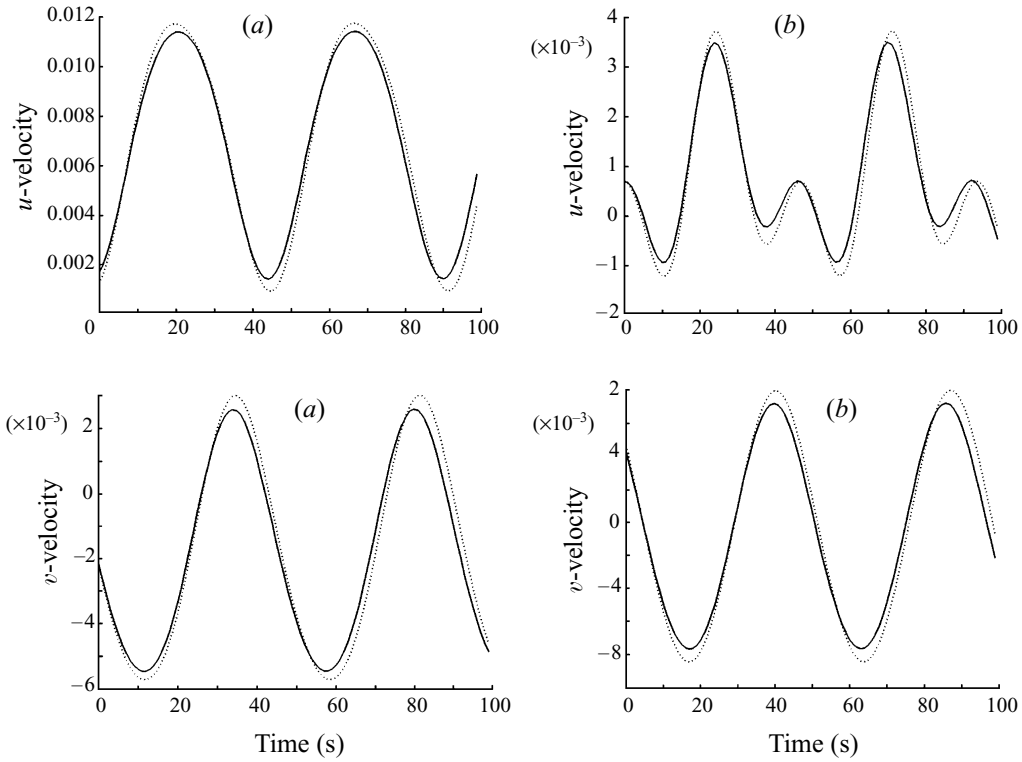


FIGURE 8. Comparison between CFD flow (dotted lines) and prototype model (solid lines): velocity at points (*a*) and (*b*) of figure 9

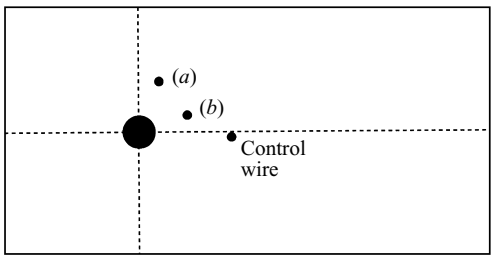


FIGURE 9. Geometry of cylinder, control wire and two velocity sensors.

lines are the mode amplitudes predicted by the unforced prototype, and the dotted lines are those measured directly from the CFD data ensemble. The model predicts a Strouhal number just 2% greater than that observed from the CFD integration of the wake and the maximum mode amplitudes are also predicted accurately. A reconstructed time series for velocity signals at two different points in the unforced cylinder wake is shown in figure 8; the behaviour of the velocity at these two points, which is shown in figure 9, is predicted adequately. The power spectral density of a 512 point Hanning windowed time series of the velocity signals calculated from the flow prototype can be compared to that of the original CFD solution in figure 3. The figure shows the predicted natural shedding frequency and three higher harmonics of the prototype flow.

For the prototype model to be of use in testing the feasibility of the control scheme,

https://doi.org/10.1017/S0022112098002122 Published online by Cambridge University Press

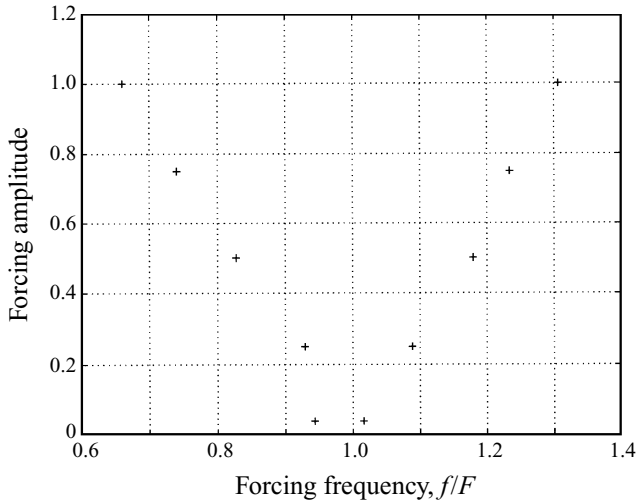


FIGURE 10. Example of prototype forcing entrainment region.

however, the response of the prototype to external control forcing has to be correct, at least qualitatively. After integration of the prototype, with harmonic control inputs (each mode is perturbed by a different amount corresponding to the inner product of each mode with the forcing in equation (13)), qualitative agreement with some of the aspects of experimental cylinder wakes is found. During periodic forcing, the prototype flow is characterized by lock-in states and non-lock-in states analogous to those that are observed in actual cylinder wakes (Karniadakis & Triantafyllou 1989; Detemple-Laake & Eckelmann 1989). Figure 10 shows points on the boundary between lock-in and non-lock-in states for the prototype flow model. The points on the figure are the points in control frequency and amplitude phase space where the wake oscillations cease to have a single set of peaks in the power spectrum of velocity signals. The frequency axis is normalized by the natural shedding frequency. The figure therefore represents a lock-in region, or region of entrainment, for periodic forcing of the prototype flow and is in qualitative agreement with the entrainment regions observed in experimental, forced cylinder wakes (Olinger & Sreenivasan 1988), high-order numerical simulations of forced cylinder wakes (Karniadakis & Triantafyllou 1989) and entrainment regions predicted by other low-dimensional wake models (Ohle & Eckelmann 1992). Entrainment regions, which are some of the most significant features of the forced cylinder wake (Olinger & Sreenivasan 1988), are modelled adequately by the prototype (only a qualitative agreement is necessary for initial testing of the control strategy). The temporal behaviour of the forced prototype flow is therefore also in agreement with experiment.

The spatial structure of the forced prototype is less representative of an actual cylinder wake because the prototype consists of only four spatial modes: many more modes are necessary for the spatial characterization of all of the flow features resulting from external perturbation of the wake. The ability of the prototype model to encapsulate the forced spatial structures of the flow, rather than just the temporal features, is of interest. The stationary POD basis encapsulates a small region of the forced phase space (i.e. the region corresponding to the growth of von Kármán shedding). The POD modes satisfy the flow boundary conditions (the control input is significant in the near wake but is almost zero on the domain boundaries. The control

https://doi.org/10.1017/S0022112098002122 Published online by Cambridge University Press

input is therefore consistent with the boundary conditions) and the POD modes are orthonormal and satisfy incompressibility. The stationary POD basis can therefore be expected to provide some degree of approximation to other flow features outwith the characterization ensemble (Sirovich 1987) (for example, features of forced flow). However, in the literature, a POD basis consisting of only six modes was deficient at representing a cylinder wake flow at off reference Reynolds numbers in Deane *et al.* 1991 (mainly because of the differences in mean flow between different Reynolds number wakes). The four-mode, stationary POD basis can thus be expected to provide only a crude approximation to the velocity fields of forced, non-stationary flows.

In summary, the prototype flow model: produces, with little computational effort, velocity fields that predict, quantitatively, the spatio-temporal growth of von Kármán vortex shedding behind the cylinder; predicts, quantitatively, the spatio-temporal behaviour of the cylinder wake during natural limit cycle oscillations; and predicts, qualitatively, the temporal response of the cylinder wake to excitation. The prototype also contains a degree of spatial complexity (i.e. global flow oscillations are not always recordable from any single coordinate). The predictions are in agreement with experimental observations of cylinder wakes and with higher-order simulations (Karniadakis & Triantafyllou 1989; Ohle & Eckelmann 1992; Noack *et al.* 1992; Olinger & Sreenivasan 1988; Noack & Eckelmann 1992; Deane *et al.* 1991).

5. Control of the prototype cylinder wake

5.1. *Controller mode extraction*

The first step in the control strategy is determination of the principal POD modes of the non-stationary prototype velocity fields (obtained from the forced prototype) with a linear neural network tool. The velocity fields of the prototype flow are sampled at a lower spatial resolution than that of the prototype and random, uniformly distributed, noise is added to the measured velocity fields, to simulate experimental uncertainty. The network data ensemble therefore consists of a series of noisy, low-resolution, velocity fields of the forced prototype flow, from which the first two 'non-stationary' modes are extracted for use by the control scheme. These 'non-stationary' modes are termed *controller modes*. The mode extraction is performed on a section of the near wake of the cylinder using a 40×15 regular, Cartesian grid, rather than the 110×60 irregular grid of the entire CFD wake – the mode extraction network is therefore presented with only limited information of the CFD wake.

The spatial noise field added to the prototype flow field is normally distributed, and mode extraction is performed on several sets of noisy flow field ensembles, with different noise variances, to determine the effect of random uncertainty on the mode extraction network. This corruption of the velocity field is used to introduce some uncertainty, which is likely to exist (in some form) in an experiment, into the flow field measurements. The random corruption is not meant to be representative of any particular fluid mechanical noise (turbulence for example is not random) but is introduced to check the robustness of the characterization and control strategy. (The actual sources of noise in an experimental flow derive from environmental, acoustic noise, electrical noise in measurement apparatus, transition to turbulence and if, for example, smoke flow is used to visualize the flow, then uncertainty is introduced because the smoke particles do not follow the flow exactly.) The mean (training ensemble average) flow field is subtracted from each member of the ensemble, which is then characterized by the POD.

https://doi.org/10.1017/S0022112098002122 Published online by Cambridge University Press

The structure of the velocity field is affected adversely by addition of the noise, but the first two modes developed for velocity fields that are noise-free, or have a medium or high noise variance show no significant differences: the lower energy modes are neglected and so the POD mode extraction process acts as a noise filter and extracts only large-scale coherent structure, neglecting the noise which has low energy and is uncorrelated.

The time-varying mode amplitudes are output by the mode extraction network on input of a time-dependent velocity field.

5.2. *Nonlinear prediction of the prototype flow response*

The observed response of the controller modes to excitation of the prototype flow is used to train a nonlinear neural network emulator that forms the core of the control strategy. The prototype flow is subjected to uniformly distributed, random bursts of control input at various amplitudes. The control input is discrete, and each control input lasts for a tenth of a flow period. After the addition of the control the prototype flow is integrated for one tenth of a flow period and the flow field is measured and input, along with random uncertainty, to the mode extraction network. The mode extraction network supplies the controller mode values after the addition of the control input. The training ensemble for the neural emulator consists of a time series of present controller mode amplitudes (measured from a velocity field ensemble with a medium noise level), the value of the present control, and the future controller mode amplitude after one tenth of a flow period. The emulator time step, of one tenth of a flow period, is chosen to be reasonably small to provide accuracy but large enough so that a linear model of the flow would not suffice. It is preferable that the time step is reasonably large (a real controller requires a finite time within the time-step value to perform computations and actuate the control mechanism). The amplitude range of the control input is, however, limited to a small finite value as would be the case in a real flow. In a real flow the control amplitude is limited so that the unstable global modes are stabilized without modification of the mean flow and so that a higher-dimension dynamical state (turbulence for example) is not excited.

The smallest, and therefore best, network that produces results consistent with the training data is a 4/12/2 network (the network architecture is two layers of 4 and 12 neurons connected to two output neurons – see Haykin 1994 for example). For comparison, an 8/24/2 network and a 16/48/2 network are also trained to emulate the training data. The larger networks, however, take significantly longer to train. While the generalization of the 4/12/2 network is quite good, the generalization of the 8/24/2 network and the 16/48/2 network is poor (i.e. only the 4/12/2 network performs well on data outwith the training set). Because the chosen 4/12/2 network contains relatively few weights, and only predicts the system state at the next time step, network training is quite fast. The network achieves a specified error goal, such that the sum of the squared output error is less than 0.001, after 267 cycles, starting from small, random weights, through the 1000 member training ensemble. The network is trained using an adaptive learning rate, which changes to provide fast, but stable, learning, and a momentum term of 0.95 which speeds up convergence.

5.3. *Adaptive control of the prototype flow*

A small, two-layer (and hence easy to train) nonlinear network is used to provide the control input to the prototype flow and to the emulator, given the present amplitudes and a measure of the error in the applied control. The controller, being a nonlinear network, has a maximum output amplitude of ± 1 (a physical controller would

https://doi.org/10.1017/S0022112098002122 Published online by Cambridge University Press

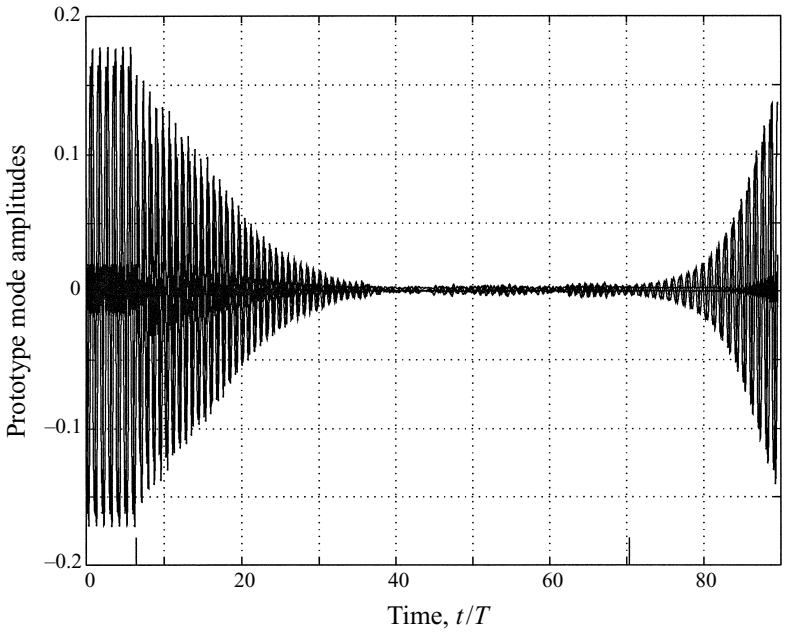


FIGURE 11. Prototype flow response during a control run: control switched on after six limit-cycle oscillations.

also have maximum actuation amplitudes). The difference between the predicted mode amplitudes and the desired zero oscillation state is backpropagated through the emulator, with its weights held fixed, and then backpropagated through the controller, whose weights are updated in order to provide a better control. The control is input to the prototype flow and the control simulation proceeds to the next time step. The controller therefore learns adaptively to provide a control that is a function of the present controller mode amplitudes and the backpropagated error between the modes and a desired state.

A typical control simulation, incorporating measurement uncertainty, is shown in figure 11. Control is switched on after six limit-cycle oscillations (delimited by the first large tick mark on the time axis). After a further 30 periods of oscillation the flow oscillations in the flow field are very small and vortex shedding is suppressed. After stabilization of the vortex shedding the control input necessary to maintain stability is only enough to stabilize disturbances due to the background noise in the flow. The qualitative nature of the control input can be compared to the experimental flow control results of (Roussopoulos 1993). The control is switched off after the second tick mark on the time axis (after approximately 600 controller steps, or a further 64 flow periods). The oscillations grow exponentially after switching off the control. The prototype flow field that results from the control scheme is seen to be almost indistinguishable from the mean flow (figure 13). The control time history is shown in figure 12. The control input is markedly nonlinear at the start of the control run, when the mode amplitudes are large, but is almost harmonic towards the end of the run, when the mode amplitudes are small. The initial nonlinear control suggests that a linear control method would take longer to control the flow. The controller, in this prototype wake, demonstrates nonlinear feedback in the early stages of control. This accords with what is known about wake dynamics: although the flow instability is

https://doi.org/10.1017/S0022112098002122 Published online by Cambridge University Press

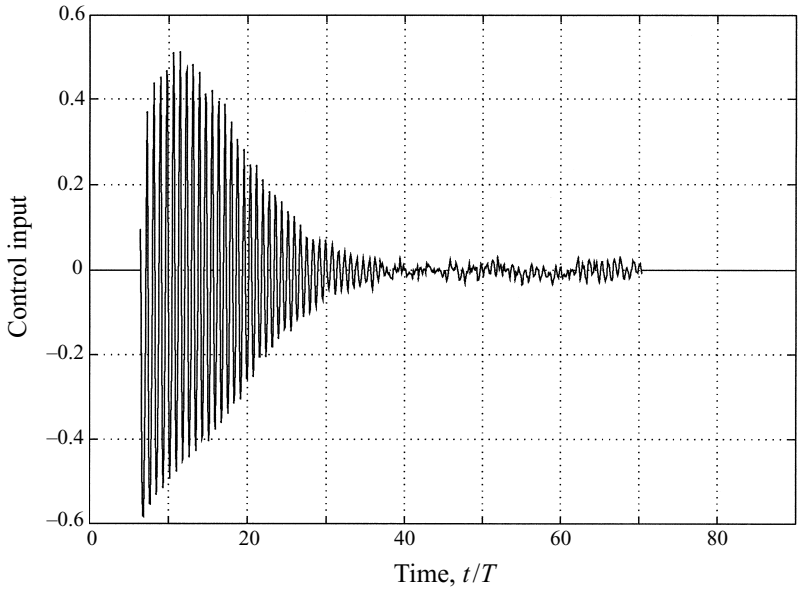


FIGURE 12. Control input during a control run: control switched on after six limit cycle oscillations.

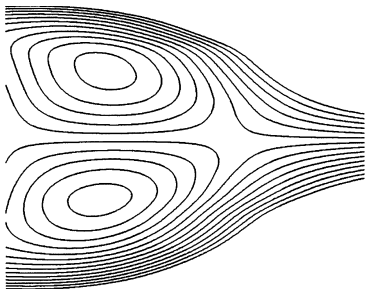


FIGURE 13. Streamlines of prototype wake immediately behind cylinder after successful suppression of oscillations.

linear, the Kármán street is a saturated nonlinear state and behaves like a nonlinear forced oscillator. Indeed a similar control strategy based on a linear emulator and linear controller takes significantly longer to suppress the flow than the nonlinear scheme.

6. Conclusions

This paper describes a scheme for control of global flow oscillations in a low Reynolds number two-dimensional cylinder wake. Active control of self-excited wake oscillations that are the result of global instability is not, in general, possible via single-sensor linear feedback. The inability of single-sensor feedback to control such absolutely unstable wakes is exemplified by numerical and experimental results of single-sensor control schemes: oscillations may be stabilized at the sensor location but exacerbated elsewhere by the destabilization of further global modes. Single-sensor control cannot stabilize all of the global modes. Multiple-sensor control of such absolutely unstable flows is therefore appropriate. A control strategy based on

https://doi.org/10.1017/S0022112098002122 Published online by Cambridge University Press

the feedback of multiple (spatially distributed) measurements of the oscillating wake would be complex and computationally slow. It is reasonable to assert that a control strategy which is based on a low-dimensional description of the flow features would be simpler and therefore computationally feasible.

A nonlinear, low-dimensional model with an artificial forcing term is used as a prototype absolutely unstable flow. The prototype flow achieves good agreement with unforced cylinder flow solutions obtained by high-order numerical simulation. The prototype also captures some of the qualitative features of experimental, forced cylinder wakes. The prototype is used to produce artificial, or simulated, non-stationary velocity fields for characterization by the controller. The controller is assumed to have only limited information about the flow (i.e. it is given lower-resolution, noisy data and only two controller modes, rather than four modes, are extracted). Nevertheless, the nonlinear emulator predicts the flow dynamics successfully and the nonlinear controller suppresses the oscillations representative of vortex shedding.

Successful control of a simplified prototype wake has demonstrated the feasibility of the control strategy for spatially complex, self-excited wake flows like the circular cylinder. The control is robust to external perturbations and noisy velocity field measurements.

The controller achieves stabilization of the prototype wake at a Reynolds number above that at which single-sensor linear control schemes fail; the extra capability of the control strategy may be attributed to the feedback of spatially distributed POD modes, rather than single-sensor measurements, and also the use of a nonlinear predictive model of the large scale flow dynamics.

The next important stage in this research is to implement the control strategy outlined in this paper on a full Navier–Stokes solution of the cylinder flow. Full numerical solution will have more spatial complexity and more POD modes will be necessary for flow characterization. It is expected that the next implemetation of the controller will be on a low Reynolds number, laminar wake (to obviate the additional complexity of three-dimensionality and turbulence). The author is currently adapting the controller to the one-dimensional complex Ginzburg–Landau equation.

Once the wake control strategy is implemented on a full Navier–Stokes solution, an experimental study may be undertaken. Experimental implemetation of the control strategy will have to address spatially distributed flow measurements (with a rake of hot wires for example, or by characterization of a smoke-seeded flow).

The author wishes to acknowledge the advice of R. B. Green and J. Anderson of the Department of Aerospace Engineering at the University of Glasgow. Part of this work was supported under EPSRC grant number GR/L59030.

REFERENCES

Berkooz, G., Psiaki, M. & Fischer, M. 1994 Estimation and control of models of the turbulent wall layer. In *Active Control of Vibration and Noise*. ASME.

Cortelezzi, L. 1996 Non-linear feedback control of the wake past a suction point. *J. Fluid Mech.* **327**, 303–324.

Cortelezzi, L., Leonard, A. & Doyle, J. C. 1994 An example of active circulation control of the unsteady separated flow past a semi-infinite plate. *J. Fluid Mech.* **260**, 127–154.

Deane, A. E., Kevrekidis, I. G., Karniadakis, G. E. & Orszag, S. A. 1991 Low-dimensional models for complex geometry flows. *Phys. Fluids* A **3**, 2337–2354.

Detemple-Laake, E. & Eckelmann, H. 1989 Phenomenology of Karman vortex streets in oscillatory flow. *Exps. Fluids* **7**, 217–227.

https://doi.org/10.1017/S0022112098002122 Published online by Cambridge University Press

Ffowcs-Williams, J. E. & Zhao, B. C. 1989 The active control of vortex shedding. *J. Fluids Struct.* **3**, 115–122.

Gillies, E. A. & Anderson, J. 1994 Low-dimensional characterization and control of non-linear flow phenomena. In *Proc. 19th ICAS Congress, Anaheim, USA.*

Glezer, A., Kadioglu, Z. & Pearlstein, A. J. 1989 Development of an extended proper orthogonal decomposition to a time-periodically forced plane mixing layer. *Phys. Fluids* A **1**, 1363–1373.

Gopalkrishnan, R., Triantafyllou, M. S., Triantafyllou, G. S. & Barret, D. 1994 Active vorticity control in a shear flow using a flapping foil. *J. Fluid Mech.* **274**, 1–21.

Haykin, S. 1994 *Neural Networks: a Comprehensive Foundation*. Macmillan.

Holmes, P., Lumley, J. & Berkooz, G. 1996 *Turbulence, Coherent Structures, Dynamical Systems and Symmetry*. Cambridge University Press.

Huerre, P. & Monkewitz, P. A. 1990 Local and global instabilities in spatially developing flows. *Ann. Rev. Fluid Mech.* **22**, 473–537.

Hush, D. R. & Horne, B. G. 1993 Progress in supervised neural networks. *IEEE Signal Processing Magazine* .

Jacobson, S. A. & Reynolds, W. C. 1993 Active control of boundary layer wall shear stress using self-learning neural networks. *AIAA Paper* 93-3272.

Karniadakis, G. E. & Triantafyllou, G. S. 1989 Frequency selection and asymptotic states in laminar wakes. *J. Fluid Mech.* **199**, 441–469.

Kim, S. W. & Benson, T. J. 1992 Comparison of the SMAC,PISO and iterative time-advancing schemes for unsteady flows. *J. Computers Fluids* **21**, 435–454.

Lewit, M. 1992 Active control of dipole sound from cylinders. In *Proc. DAGA 1992, Berlin Germany*.

Lightbody, G., Wu, Q. H. & Irwin, G. W. 1992 Control applications for feedforward neural networks. In *Neural Networks for Control and Systems*. Peregrinus.

Metcalfe, R. W., Rutland, C. J., Duncan, J. H. & Riley, J. J. 1986 Numerical simulations of active stabilization of laminar boundary layers. *AIAA J.* **24**, 1494–1501.

Monkewitz, P. A. 1989 Feedback control of global oscillations in fluid systems. *AIAA Paper* 89-0991.

Nguyen, D. H. & Widrow, B. 1990 Neural networks for self-learning control systems. *IEEE Control Systems Magazine*.

Noack, B. R. & Eckelmann, H. 1992 On chaos on wakes. *Physica* D **56**, 151–164.

Noack, B. R., Ohle, F. & Eckelmann, H. 1992 Construction and analysis of differential equations from experimental time series of oscillatory systems. *Physica* D **56**, 389–405.

Ohle, F. & Eckelmann, H. 1992 Modelling of a von Karman vortex street at low Reynolds numbers. *Phys. Fluids* A **4**, 1707–1714.

Olinger, D. J. & Sreenivasan, K. R. 1988 Non-linear dynamics in the wake of an oscillating cylinder. *Phys. Rev. Lett.* **60**, 797–800.

Park, D. S., Ladd, D. M. & Hendricks, E. W. 1994 Feedback control of von Karman vortex shedding behind a cylinder at low Reynolds numbers. *Phys. Fluids* **6**, 2390–2405.

Roussopoulos, K. 1993 Feedback control of vortex shedding at low Reynolds numbers. *J. Fluid Mech.* **248**, 267–296.

Schumm, M., Berger, E. & Monkewitz, P. A. 1994 Self-excited oscillations in the wake of two-dimensional bluff bodies and their control. *J. Fluid Mech.* **271**, 17–53.

Sirovich, L. 1987 Turbulence and the dynamics of coherent structures. *Q. Appl. Maths* **45**, 561–590.

Tao, J. S., Huang, X. Y. & Chen, W. K. 1996 Flow visualization study of feedback control of vortex shedding from a circular cylinder. *J. Fluids Struct.* **10**, 965–970.

Taylor, C. & Morgan, K. 1980 *Recent Advances in Numerical Methods in Fluids*. Pineridge Press, Swansea.

Tokumaru, P. T. & Dimotakis, P. E. 1991 Rotary oscillation control of a cylinder wake. *J. Fluid Mech.* **224**, 77–90.

Williamson, C. H. K. 1996 Vortex dynamics in the cylinder wake. *Ann. Rev. Fluid Mech.* **28**, 477–539.

https://doi.org/10.1017/S0022112098002122 Published online by Cambridge University Press